Journal of the Brazilian Society of Mechanical Sciences and Engineering (2020) 42:89
https://doi.org/10.1007/s40430-020-2169-x

TECHNICAL PAPER

Dielectrophoretic microfluidic device for separation of red blood cells and platelets: a model-based study

Yaolong Zhang[1] · **Xueye Chen**[1]

Received: 8 April 2019 / Accepted: 31 December 2019

Abstract
The paper proposes a dielectrophoresis microfluidic chip for particle separation, which uses dielectric properties to perform size-based fractionation of red blood cells and platelets. Based on the control variables, the distribution of the electric field in the chip and the trajectory of the particles in the microfluidic channel are calculated using COMSOL Multiphysics under different electrode shapes, voltages and chip exit structures. Both red blood cells and platelets respond to negative dielectrophoresis at an alternating current signal with a frequency of 100 kHz. The larger red blood cells are subjected to a stronger dielectrophoretic force than the platelets and are biased toward the right outlet, and the platelets flow out from the left outlet under the combined action of fluid force and dielectrophoretic force to achieve the purpose of separation. On this basis, through quantitative comparison and analysis, a more optimized microfluidic chip capable of effectively separating particles is finally selected.

Keywords Comsol · Dielectrophoresis · Microfluidic chip · Particle separation

1 Introduction

The main function of platelets (PLTs) is coagulation and hemostasis, repairing damaged blood vessels. Changes in concentration and quantity can directly or indirectly indicate changes in human organ function and disease occurrence. Low platelet concentrations can cause bleeding, while high concentrations can lead to thrombosis and related complications such as infarction or stroke [1]. Therefore, we need to pay attention to the detection of its concentration at all times, in order to facilitate treatment in advance. First, PLTs need to be separated from the blood. With the rapid development of MEMS-related technologies [2, 3], commonly used particle separation techniques mainly include centrifugation technology [4], fluorescence technology (FACS) [5], magnetic technology (MACS) [6] and dielectrophoresis (DEP) separation technology [7]. The microfluidic chip based on DEP technology has become an important means of particle manipulation and separation with its advantages of low loss, easy integration, low cost and rapid separation [8–10] and has important practical value. By using the fact that PLTs are the smallest cells in the blood, it is possible to use dielectric properties to perform size-based fractionation of particles in the blood.

After some investigation, we found that some people have done research on this aspect [11–13]. Haider et al. [14] designed a microfluidic device with three outlets for continuous separation of blood cells and studied the effects of different outlet designs, number of intake units (population ratio) and buffer flow on blood cell separation efficiency. Bobby et al. [15–17] used a microfluidic device with staggered transducer electrodes at the bottom of the channel to study a series of parametric studies including electrode/gap length. Parham et al. [18] proposed a microfluidic device with four triangular electrodes to continuously focus and separate living and dead cells as well as polystyrene particles. Under an optimum condition, an efficiency of approximately 100% was obtained. Barbaros et al. [19] compared the point-particle approach and finite-sized particle approach and the demonstration of the particle–particle interaction for several DEP applications in microchannel settings. This paper improves the parameters and structure of the separation chip based on the previous design. By referring to various kinds of the literature, the effects of different structure

Technical Editor: Erick de Moraes Franklin, Ph.D.

✉ Xueye Chen
xueye_chen@126.com

[1] Liaoning University of Technology, Jinzhou 121001, China

Published online: 17 January 2020

and shape electrodes, different voltages and different chip exit structures on particle manipulation separation were simulated. The aim is to improve the separation efficiency of red blood cells (RBCs) and platelets (PLTs) by optimizing the design of the separation chip. This paper selects a model based on the work of the predecessors. The model utilizes the characteristics of double electrophoresis in fluid flow gap particle tracking to successfully achieve continuous separation of PLTs and RBCs.

2 Theoretical concept

The dielectrophoretic force is generated because the dielectric particles placed in a non-uniform electric field are polarized to generate corresponding induced charges on the surface [20], which in turn generates dipole moments, and the ends of the positive and negative charges of the particles are uneven due to the force. And the corresponding movement occurs. In this paper, we will analyze the mechanism of particle separation by using the different negative dielectrophoretic forces of RBCs and PLTs, calculate the size of the dielectrophoretic force and analyze the main factors affecting DEP.

DEP is the movement of particles in a non-uniform electric field due to the interaction of the particles' induced dipoles with the spatial gradient of the electric field norm. In a sinusoidally varying electric field, the form is [21]:

$$F_{\mathrm{DEP}} = 2\pi r^3 \varepsilon_0 \varepsilon_{\mathrm{m}} \mathrm{Re}[K(\omega)] \nabla E^2 \tag{1}$$

$$K(\omega) = \frac{\varepsilon_{\mathrm{p}}^* - \varepsilon_{\mathrm{m}}^*}{2\varepsilon_{\mathrm{m}}^* + \varepsilon_{\mathrm{p}}^*}, \quad \varepsilon^* = \varepsilon + \frac{\sigma}{i\omega} \tag{2}$$

where ε_0 and ε_{m} are the vacuum permittivity and the permittivity of the suspending medium and $\varepsilon_{\mathrm{m}}^*$and $\varepsilon_{\mathrm{p}}^*$ are complex permittivity of the suspending medium and the particle, respectively. E represents the root-mean-squared electric field strength, and Re[$K(\omega)$] represents the real part of the Clausius–Mossotti (CM) factor. ω is the frequency of the applied electric field. ε and σ are the permittivity and conductivity of the material.

Among them, Re[$K(\omega)$] varies between [− 0.5, 1]. When Re[$K(\omega)$] is positive, the particle moves to the region with high electric field strength, called positive dielectrophoresis (pDEP); when Re[$K(\omega)$] is negative, the particle moves to the region with low electric field strength, called negative dielectrophoresis (nDEP).

Cells generally have a relatively complex internal structure that can affect the dielectric properties of cells, and equivalent cells of different structures produce different results. Some can be directly equivalent to a solid sphere, and some need to establish an equivalent model for biological particles. Among them, the concentric spherical model is more common.

First, the simplest modeling is the single spherical model, whose effective dielectric constant is $\varepsilon_{\mathrm{eq}}$* [22]:

$$\varepsilon_{\mathrm{eq}}^* = \varepsilon_{\mathrm{s}}^* \frac{\left(\frac{r_0}{r_i}\right)^3 + \frac{2\left(\varepsilon_{\mathrm{p}}^* - \varepsilon_{\mathrm{s}}^*\right)}{\varepsilon_{\mathrm{p}}^* + 2\varepsilon_{\mathrm{s}}^*}}{\left(\frac{r_0}{r_i}\right)^3 - \frac{2\left(\varepsilon_{\mathrm{p}}^* - \varepsilon_{\mathrm{s}}^*\right)}{\varepsilon_{\mathrm{p}}^* + 2\varepsilon_{\mathrm{s}}^*}} \tag{3}$$

where r_0 and r_{i} (SI units: m) are the outer and inner radii of the shell, respectively; ε_{p}* is the complex permittivity of the particles, and ε_{s}* is the complex permittivity of the outer shell. When calculating the dielectrophoretic force, the complex permittivity ε_{p} of the particle is replaced by the equivalent complex permittivity $\varepsilon_{\mathrm{eq}}$* of the uniform particle composed of the shell and the interior of the particle. The model used in this paper is a single spherical model.

It can be seen from the dielectrophoretic force formula that F_{DEP} is the force determined by r^3, Re[$K(\omega)$] and E^2. The amount of dielectrophoretic force that a particle receives is proportional to its radius, and particles with a larger radius are subjected to a dielectrophoretic force greater than that of a smaller particle. The frequency used in this work was 100 kHz, and the dielectric conductivity was 55 ms/m. At this time, the Clausius–Mossotti factor of both RBCs and PLTs is negative, as shown in Fig. 1. Both particles are subjected to nDEP, and because of the difference in size (the volume of red blood cell is about 10 times that of platelet), the dielectrophoretic force of RBCs is much stronger than that of PLTs, thus achieving the purpose of separation.

In the modeling of the particle flow, the fluid flow rate is very low, the fluid is mainly affected by the viscous force, and the inertial force is negligible. In the normal temperature and pressure environment, the force caused by Brownian motion is small and has little effect on the research. In addition, the particle density is similar to the fluid density, and the particles stay in the channel for a short period of time, so that the sedimentation of the particles in the vertical direction can be ignored. Therefore, the dielectrophoretic force and fluid viscous force will be mainly considered when investigating the force movement of particles in this system. Trajectory of the microscale entity is described as:

$$m\ddot{x}(t) + K_f \dot{x}(t) = F_{\mathrm{DEP}}(x, E, t) \tag{4}$$

$$K_f \dot{x}(t) = 6\pi r \mu v \tag{5}$$

$$x(t) = \left[x, y\right]^{\mathrm{T}} \tag{6}$$

where m represents the mass of the particle and $x(t)$ is the position of the particle in the vertical coordinate system. $K_f\dot{\mathbf{x}}(t)$ is the linear viscous resistance, μ represents the

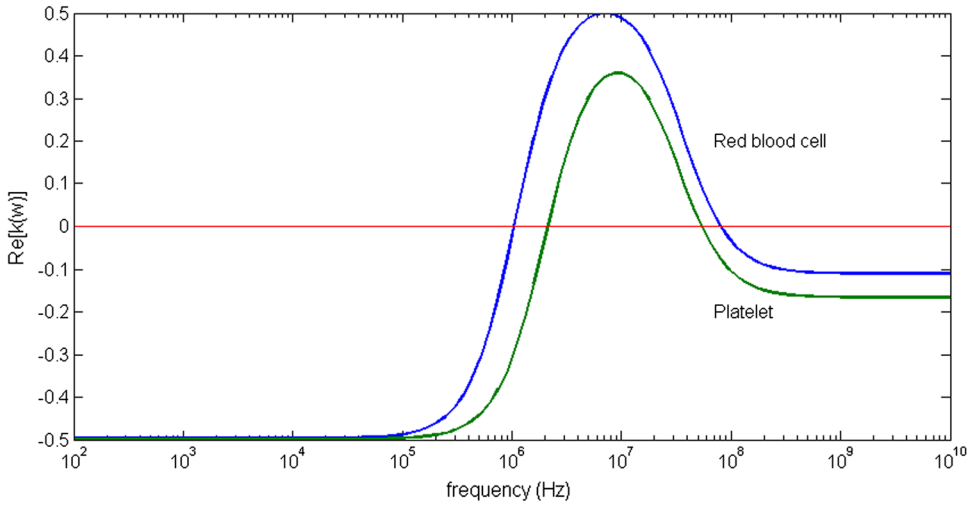

Fig. 1 The real part of the Clausius–Mossotti factor

dynamic viscosity coefficient, and v is the velocity of the particles relative to the fluid.

The performance of the device is quantified by separation efficiency (SE) [see (7) below], separation purity (SP) [see (8) below] [23] and the time required to complete the separation.

$$\mathrm{SE}(A) = \frac{\text{of entities of type A appearing at target outlet of A}}{\text{of entities of type A introduced at intlet}} \tag{7}$$

$$\mathrm{SP}(A) = \frac{\text{of entities of type A appearing at target outlet of A}}{\text{of entities of all types appearing at target outlet of A}} \tag{8}$$

3 Model and design

In the previous analysis, the basic formula of the dielectrophoretic force of the particles in the microchannel is obtained. Next, we will analyze the factors that may affect the separation efficiency from the principle of DEP, simulate the potential, electric field and particle trajectory at any point in the microchannel under various conditions and compare the results of the final particle separation to determine a more scientific, reasonable and efficient microfluidic chip.

3.1 Two-dimensional simulation model of chip

In the model used here, the electrode extends over the entire width of the microchannel, and the particles have no F_{DEP} effect along the width of the channel. Moreover, in the sections along the height direction of the channel, the potential distribution is the same, so the three-dimensional model can be simplified into a two-dimensional model for simulation. The basic two-dimensional geometry of the device used in this topic is shown in Fig. 2.

The chip design consists of three distinct sections: two inlets, two outlets and a separate region, wherein the nonuniform electric field generated by the arrangement of electrodes of alternating polarity changes the particle trajectory.

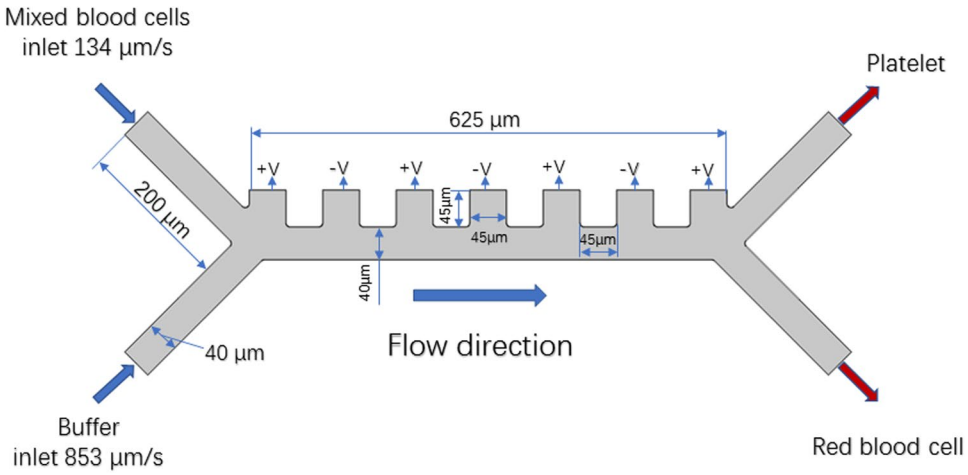

Fig. 2 2D geometric model of the modeling device

RBCs and PLTs enter the chip from the left inlet, and the carrier fluid enters the chip from the right inlet. The separation zone microchannel has a width of 40 μm and a length of 625 μm. The inlet and outlet channels are 200 μm long, 40 μm wide and have an electrode width of 45 μm and an interval of 45 μm. As shown above, the inlet velocity of the right inlet (853 μm/s) is significantly higher than the left inlet (154 μm/s), thereby focusing all of the injected particles onto the left portion of the chip. The frequency used in this work is 100 kHz, and the carrier fluid conductivity is 55 ms/m. At this time, both RBCs and PLTs undergo nDEP, but due to size differences, the dielectrophoretic force of RBCs is much stronger than that of PLTs. Dielectrophoretic forces repel larger RBCs such that they appear in the channels of the right outlet, while smaller PLTs appear in the channels of the left outlet under the combined action of dielectrophoretic and fluid forces. The parameters of the two types of cells are shown in Table 1.

In this paper, the finite element analysis software COMSOL Multimechanics is used for simulation analysis. COMSOL Multiphysics is a large-scale multi-physical field coupled with numerical simulation software. It is based on the finite element method to realize the simulation of real physical phenomena by solving partial differential equations (groups). It is applied to the research and engineering calculation of various disciplines, simulating the physical processes of science and engineering.

In this paper, the laminar flow module, AC/DC module and particle trajectory tracking module in the software are used to simulate the separation process. The laminar flow module is used to calculate the distribution of the flow field in the main channel. AC/DC module is used to calculate the distribution of the electric field in the main channel. Particle trajectory tracking module coupling the influence of the flow field and electric field on the particle trajectory is used to calculate the trajectory of the particles in the channel.

3.2 Numerical simulation methods and boundary conditions

The flow field distribution and electric field distribution in the channel are solved in the laminar flow module and the AC/DC module, and the Navier–Stokes equation and the Laplace equation are used as the governing equations, respectively.

3.2.1 Flow modeling

In a microfluidic system, laminar flow corresponds to the flow with small Re (Re < 1), the viscosity term of the Navier–Stokes equation dominates, and the inertia term can be ignored. The inertial forces are small compared with the viscous forces. Therefore, the inertial term in the Navier–Stokes equations can be neglected. The governing equations of Stokes flow for the conservation of momentum and the continuity equation for the conservation of mass are as follows:

$$\nabla \cdot \left[-pI + \mu\left(\nabla u + (\nabla u)^{\mathrm{T}}\right)\right] + F = 0 \tag{9}$$

$$\rho \nabla \cdot (u) = 0. \tag{10}$$

At this point, the corresponding boundary conditions are: (1) The channel wall is a nonslip boundary. (2) The inlet fluid is controlled by the flow rate, and the flow rates of the left and right inlet are 134 μm/s and 853 μm/s, respectively. (3) The fluid at the outlet is controlled by the pressure, and the pressure at the outlet is set to be atmospheric pressure, that is, $P = 0$.

3.2.2 Electric field modeling

Under steady-state conditions, the electric field distribution within the microchannel is controlled by the Laplace equation:

$$\nabla \cdot J = Q_i \tag{11}$$

$$J = \sigma E + J_e \tag{12}$$

$$E = -\nabla V. \tag{13}$$

At this point, the corresponding boundary conditions are: (1) The wall surface, inlet and outlet of the microchannel are insulated boundary conditions. (2) The potential on the electrode is constant.

3.2.3 Blood cells and DEP modeling

Using the particle tracking module in COMSOL, you can predict the trajectory of particles in the channel. The

Table 1 Dielectric properties of two types of cells

Cells	Radius (μm)	Conductivity (ms/m)	Relative permittivity	Conductivity of the shell (ms/m)	Relative permittivity of the shell	Shell thickness (nm)
Platelets	0.9	0.25	50	1E−6	6	8
Red blood cells	2.5	0.31	59	1E−6	4.44	9

dielectrophoretic force and the Stokes force applied to the particles are obtained by solving the electric field and the flow field, respectively. The governing equations for F_{DEP} are given in Eqs. (1) and (2). At the same time, the single-cell model is used for blood cell particles, and the governing equation is given by Eq. (3). At this point, the corresponding boundary conditions are:

(1) The channel wall condition is rebound. (2) The initial velocity of the inlet fluid is based on the velocity field in the laminar flow. (3) The drag force follows Stokes' law.

3.3 Grid selection and independence test

The microfluidic device is discretized in this paper using a triangular and boundary layer mesh element type. In this simulation, we mainly focus on the effect of particle separation, which is closely related to the electric field distribution and fluid velocity in the channel. Therefore, the network-independent verification is performed by taking the electric field distribution and the velocity distribution at the positions as shown in the figure, respectively.

Here, we choose to test the independence of four different grid numbers, and the results are shown in Fig. 3. The horizontal axis in the figure is the arc length, indicating the position selected in Fig. 4.

It can be seen from the figure that the number of meshes has little effect on the simulation results of the electric field distribution in the channel. Relatively speaking, the number of meshes has a certain influence on the fluid velocity; it can be seen from the magnified image, the red curve is closer to the black curve, and which corresponding grid number is 7894. Considering the calculation time and simulation error, the paper finally chooses to divide the mesh into 7894 units for simulation. The parameters of the selected grid are shown in Table 2.

4 Results and discussion

Based on the above model, the paper discusses in the case of different electrode shapes (planar, semi-circular and micro-pointed), different electrode voltages (3 V, 5 V and 7 V) and different exit angles (45°, 90° and 135°), the separation of the particles in the chip, thereby optimizing the chip step by step, determines the final structural parameters of the chip.

4.1 Experimental verification

The correctness of the research method used in this paper was verified by comparing the simulation results with the experimental results of Piacentini et al. [11]. Piacentini et al. used a 40-μm-wide electrode for particle separation. The particle trajectories of PLTs and RBCs are calculated here and compared with the experimental results in the literature, as shown in Fig. 5. It can be found that the numerical calculation results are in good agreement with the particle trajectory calculation results in the experiment. Therefore, the correctness of the numerical method we used is verified.

4.2 Electrode shape design

In this device, the manipulation of the particles is largely dependent on the design of the electrode shape. The non-uniform electric field on the microfluidic chip is mainly generated by the electrodes, so the shape and distribution of the electrodes are decisive for the distribution of F_{DEP}. This paper chooses to discuss three relatively common shapes of electrodes, namely planar, semi-circular and micro-pointed [24–26]. The Comsol simulation software is used to simulate the potential of the device, the electric field and the particle trajectory of the whole process in the case of electrodes with different shapes.

By means of the upper potential profile (Fig. 6), we can clearly see that each shape electrode has a similar potential distribution law at the same voltage (here 5 V is selected), that is, the electrode arrangement of alternating polarity produces a non-uniform electric field, thereby the particles in it are subjected to dielectrophoretic forces. Their corresponding electric field strength diagrams are shown in Fig. 7.

In Fig. 7, the electric field strength it represents is the origin of the dielectrophoretic repulsion of the particles away from the electrode. It can be seen that the higher gradient regions are located at the corners of the lateral electrode channels and in front of them. Here, a position that is 10 μm from the top of the transverse channel is taken as a reference to discuss the difference in electric field strength of each electrode shape chip. It can be found that the electric field strength of the micro-tip electrode is the largest at the same position, the planar electrode is the second, and the semi-circular electrode is the smallest. The reason for this is that at the same position in the channel, it is relatively closest to the micro-point electrode and relatively far from the semi-circular electrode, the closer the electrode is, the larger the electric field is naturally. The greater the electric field strength, the RBCs in which supposed to be subjected to large forces. A total of 610 blood cells were introduced, in which the ratio of RBCs to PLTs was 1:1, and five cells were released at each specific time step. Figure 8 simulates the particle trajectory results that reflect this.

It can be seen from Fig. 8 that in three cases, the SE and SP of the two types of cells in the device are both 100%. Among them, the trajectory deflection of the RBCs in the micro-pointed electrode is larger, indicating that the dielectrophoretic force is greater, and the separation effect with the PLTs is more obvious. Next, to compare the time required for the device to complete the separation in three

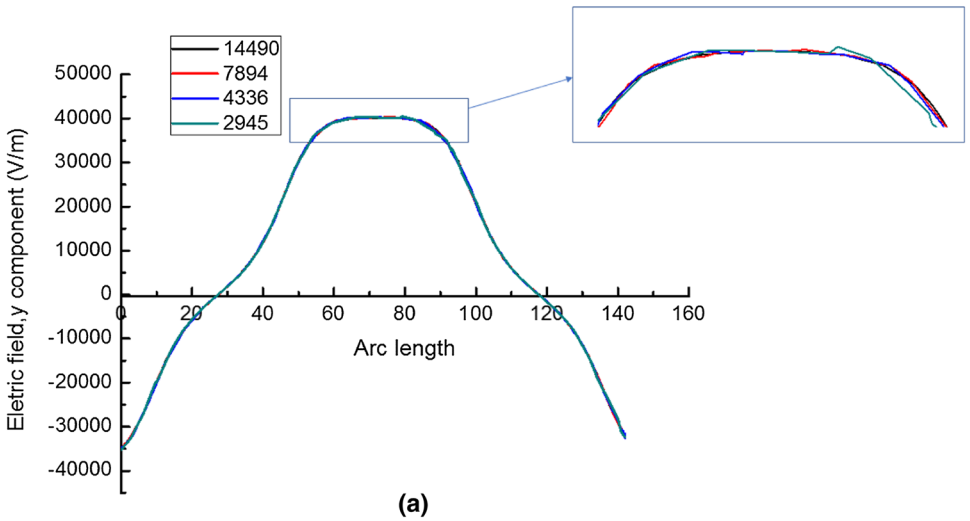

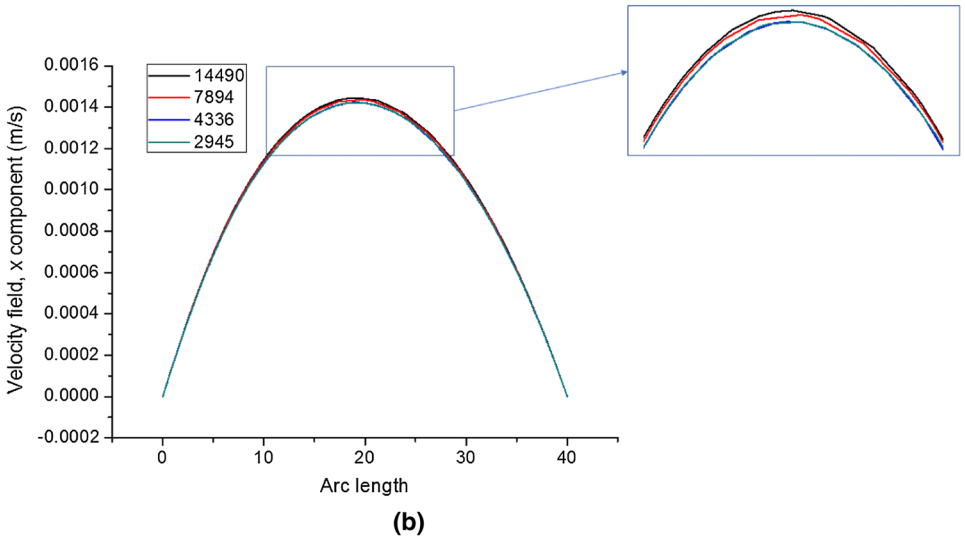

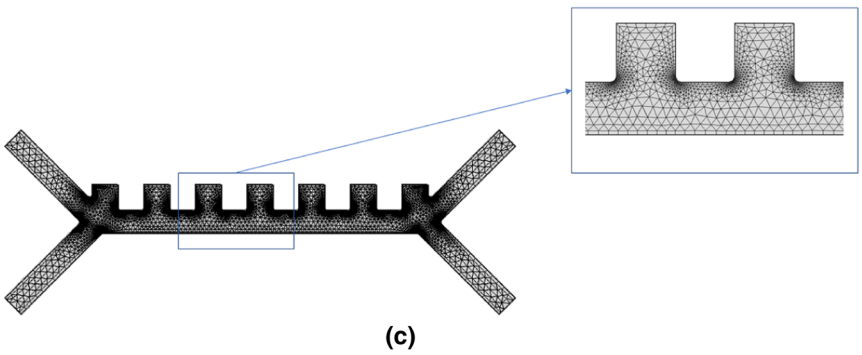

Fig. 3 Grid selection and independence test. **a** Influence of grid number on electric field distribution of selected channel locations. **b** Influence of grid number on flow field distribution of selected channel position. **c** Mesh map

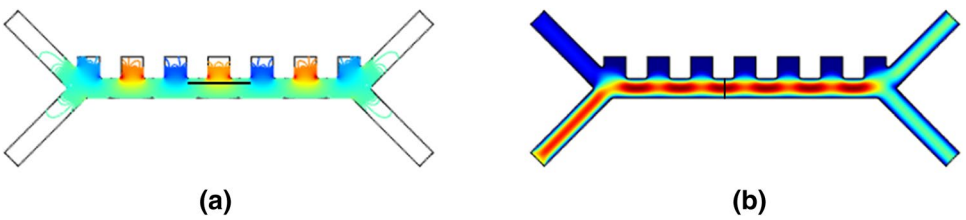

Fig. 4 Selected channel location. **a** Selected position of the electric field distribution. **b** Selected location of the flow field distribution

Table 2 Grid parameter

Grid number	The number of vertex units	The number of boundary units	The maximum cell size (μm)	The minimum cell size (μm)
14490	59	898	9	0.129
7894	59	666	14.5	0.643
4336	59	481	21.5	0.964
2945	59	377	28	1.29

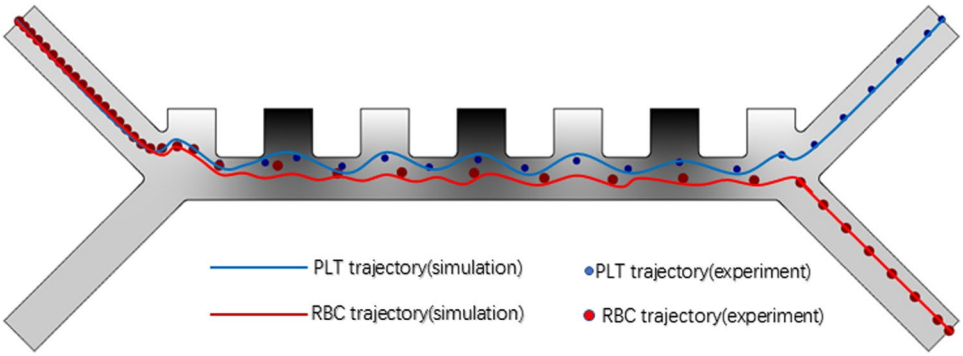

Fig. 5 PLTs and RBCs trajectories with the numerical and experimental results

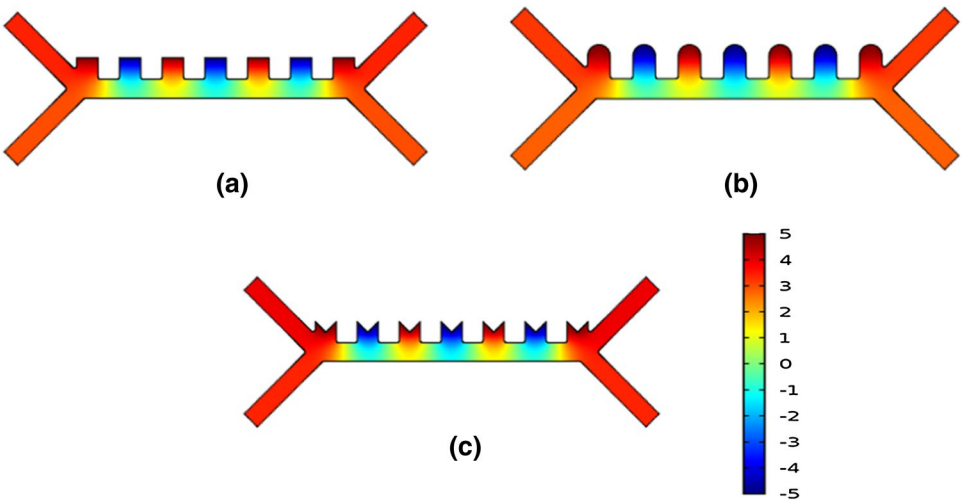

Fig. 6 Potential distribution map (V). **a** Plane electrode. **b** Semi-circular electrode. **c** Micro-pointed electrode

cases, the separation process is shown in Fig. 9. Among them, the abscissa indicates the time taken for separation, and the ordinate indicates the number of cells at the exit.

As can be seen from Fig. 9, the micro-pointed electrode chip takes the shortest time to complete the separation, with the highest separation rate and the best results. The velocity field distribution in the chip is shown in Fig. 10. It can be seen that in the chip, the closer the particles are to the center of the channel, the higher the rate. RBCs and PLTs are subjected to a large dielectrophoretic force in the micro-tip electrode chip, and the amplitude of the downward deflection is large, so the separation speed is faster. Therefore, here we select the microdots shape from the three electrode shapes.

4.3 Electrode voltage design

In addition to the shape of the chip electrode, the electric field strength can also be affected by changing the voltage applied to the electrode. Here, the separation of the particles in the micro-tip electrode chip at different voltages (3 V, 5 V, 7 V selected here) is discussed to determine a reasonable voltage, as shown in Fig. 11.

As can be seen from Fig. 11, when the electrode voltage is 3 V, the RBCs and PLTs cannot achieve effective separation because the electric field intensity is too small, and both come out from the left outlet. At this time, the SE and SP of the RBCs are SE (b) = 0% and SP (b) = 100%, respectively. The PLTs are SE (p) = 100%

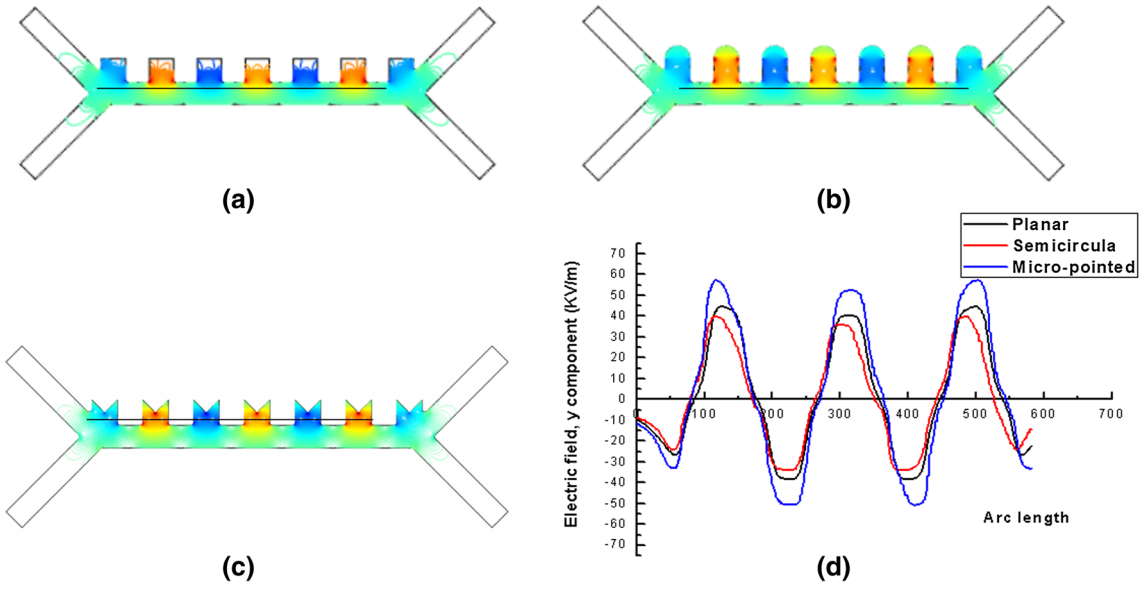

Fig. 7 Electric field intensity map (V/m). **a** Plane electrode. **b** Semi-circular electrode. **c** Micro-pointed electrode. **d** Electric field strength at the reference

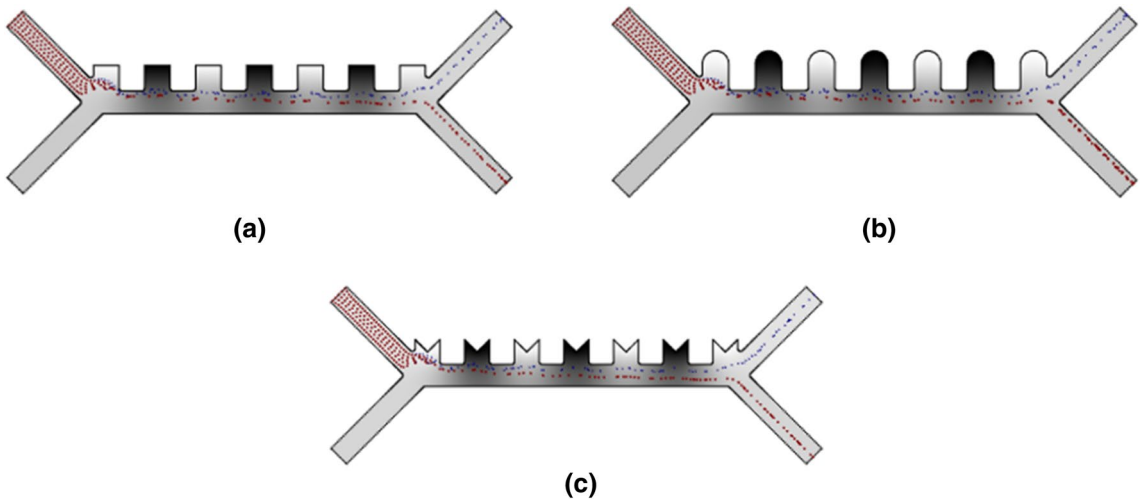

Fig. 8 Particle trajectory. **a** Plane electrode. **b** Semi-circular electrode. **c** Micro-pointed electrode

and SP (p) = 50%. When the electrode voltage is 5 V and 7 V, the SE and SP of the two types of cells in the device are both 100%. When the electrode voltage is 7 V, the RBCs deflect downward too much due to the high electric field intensity, which is far away from the center of the channel, and frictions are generated with the inner wall of the channel, affecting the separation efficiency of particles. Figure 12 shows the entire process of separating cells at 5 V and 7 V electrode voltages. It can be found that the black curve corresponding to 5 V voltage tends to be stable faster and the time required for complete cell separation is shorter. Therefore, it is more appropriate to select the 5 V electrode voltage.

4.4 Outlet design

In addition to the size of particle F_{DEP}, RBCs and PLTs appear from the same outlet in the above discussion, as shown in Fig. 11a, and RBCs contact with the inner wall of the outlet channel, as shown in Figs. 8b and 11b, affecting the separation effect and speed. Here, considering that the exit angle of the channel may have some impact on the above problems, three different exit angles (45°, 90° and

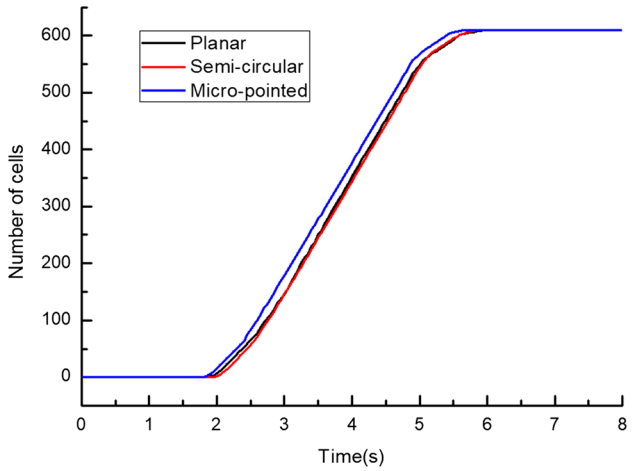

Fig. 9 Cell separation process

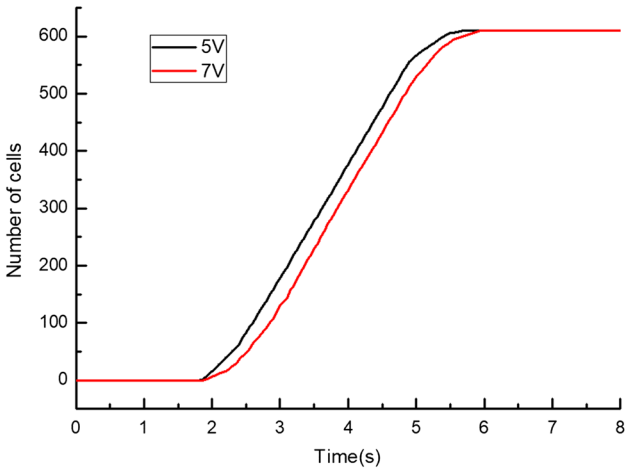

Fig. 12 Cell separation process

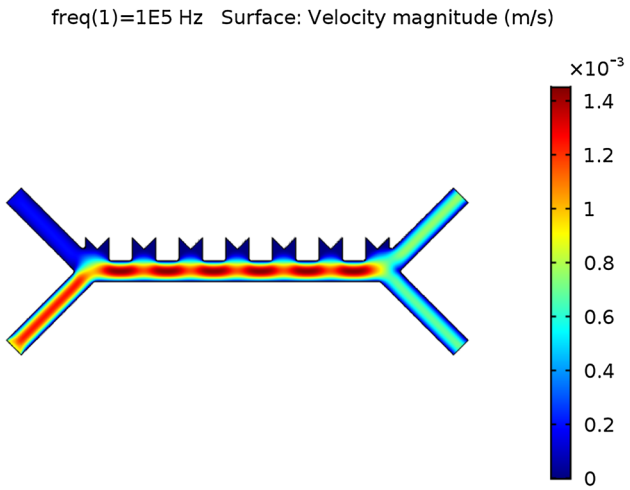

Fig. 10 Velocity magnitude (m/s)

135°) were selected to observe the particle trajectory, and the effect of the exit angle separation on the particle separation was discussed, as shown in Fig. 13.

From the particle trajectory map, it can be found that the particle separation results of the three outlet channel angles are not much different. The SE and SP of the two types of cells in the device are both 100%. Further, we quantitatively judge and select the most appropriate exit angle by statistically comparing the time required to complete the blood cell separation at each exit angle, as shown in Fig. 14.

According to the statistical results, the cells can be completely separated in three cases, and the time difference required is small. It can be seen from Fig. 14 that the black curves corresponding to the 45° exit angle are almost identical to the red curve, and relatively speaking, they reach stability faster than the blue curve, i.e., the cell separation is completed more quickly. Therefore, we finally choose a 45° exit angle.

5 Conclusion

In this paper, the principle of separation of RBCs and PLTs is theoretically analyzed and the device uses a combination of flow focusing and DEP to separate the cells depending on their size. Three different shapes of electrodes, namely planar, semi-circular and micro-pointed, are designed as experimental chips for particle separation. Several different voltages are applied to the electrodes. Three different

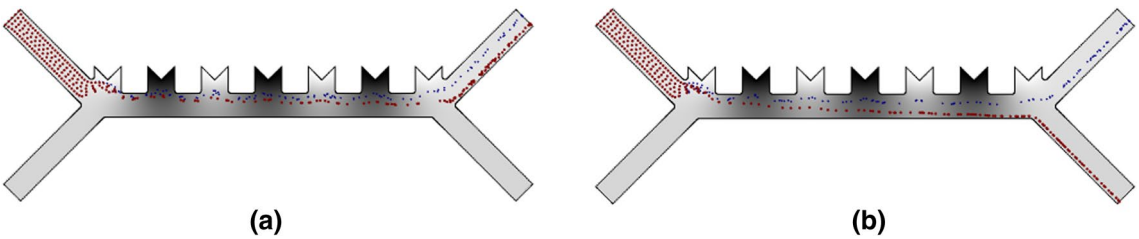

Fig. 11 Particle trajectory. **a** Voltage is 3 V. **b** Voltage is 7 V

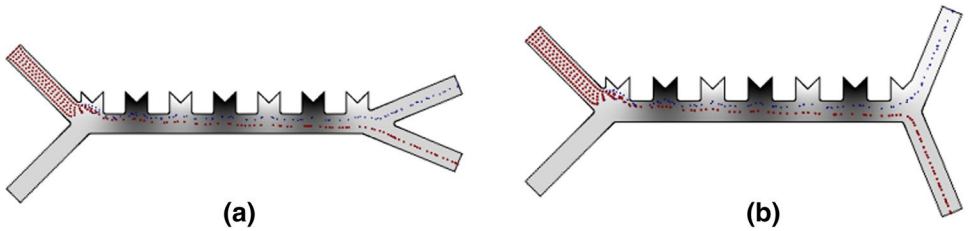

Fig. 13 Particle trajectory. **a** Exit angle is 45°. **b** Exit angle is 135°

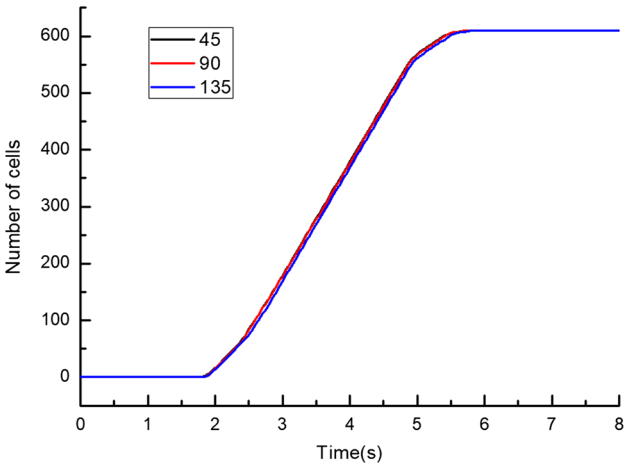

Fig. 14 Cell separation process

chip exit angles are designed. The results of the separation of RBCs and PLTs in the case of the above different combinations are simulated, and the results show that when the shape of the chip electrode is micro-pointed, the applied voltage is 5 V, and the exit angle is 45°, the separation effect is best.

Acknowledgements This work was supported by LiaoNing Revitalization Talents Program (XLYC1907122), Liaoning Natural Science Foundation (2019-MS-169). We sincerely thank Prof. Chong Liu for his kind guidance.

Author contribution All authors designed and performed the numerical simulations. The manuscript was written through contributions from all authors. All authors have given approval to the final version of the manuscript.

Compliance with ethical standards

Conflict of interest All the authors declare no conflict of interest.

References

1. Stroncek DF, Rebulla P (2007) Platelet transfusions. The Lancet 370(9585):427–438
2. Sajeesh P, Sen AK (2014) Particle separation and sorting in microfluidic devices: a review. Microfluid Nanofluid 17(1):1–52
3. Han W, Chen X, Hu Z, Yang K (2018) Three-dimensional numerical simulation of a droplet generation in a double T-junction microchannel. J Micro/Nanolithography MEMS MOEMS 17(2):025502
4. Friedman SL, Roll FJ (1987) Isolation and culture of hepatic lipocytes, Kupffer cells, and sinusoidal endothelial cells by density gradient centrifugation with Stractan. Anal Biochem 161(1):207–218
5. Raddatz MSL et al (2008) Enrichment of cell-targeting and population-specific aptamers by fluorescence-activated cell sorting. Angew Chem 120(28):5268–5271
6. Schriebl K et al (2012) Selective removal of undifferentiated human embryonic stem cells using magnetic activated cell sorting followed by a cytotoxic antibody. Tissue Eng Part A 18(9–10):899–909
7. Becker FF et al (1995) Separation of human breast cancer cells from blood by differential dielectric affinity. Proc Natl Acad Sci 92(3):860–864
8. Hughes MP (2002) Strategies for dielectrophoretic separation in laboratory-on-a-chip systems. Electrophoresis 23(16):2569–2582
9. Voldman J (2006) Electrical forces for microscale cell manipulation. Annu Rev Biomed Eng 8:425–454
10. Das D, Biswas K, Das S (2014) A microfluidic device for continuous manipulation of biological cells using dielectrophoresis. Med Eng Phys 36(6):726–731
11. Piacentini N et al (2011) Separation of platelets from other blood cells in continuous-flow by dielectrophoresis field-flow-fractionation. Biomicrofluidics 5(3):034122
12. Zheng S, Liu J-Q, Tai Y-C (2008) Streamline-based microfluidic devices for erythrocytes and leukocytes separation. J Microelectromechanical Syst 17(4):1029–1038
13. Davis JA et al (2006) Deterministic hydrodynamics: taking blood apart. Proc Natl Acad Sci 103(40):14779–14784
14. Ali H, Park CW (2016) Numerical study on the complete blood cell sorting using particle tracing and dielectrophoresis in a microfluidic device. Korea Aust Rheol J 28(4):327–339
15. Mathew B et al (2015) Modeling the trajectory of microparticles subjected to dielectrophoresis in a microfluidic device for field flow fractionation. Chem Eng Sci 138:266–280
16. Mathew B et al (2016) Path of microparticles in a microfluidic device employing dielectrophoresis for hyperlayer field-flow fractionation. Microsyst Technol 22(7):1721–1732
17. Mathew B et al (2016) Model-based analysis of a dielectrophoretic microfluidic device for field-flow fractionation. J Sep Sci 39(15):3028–3036
18. Tajik P et al (2019) Simple, cost-effective, and continuous 3D dielectrophoretic microchip for concentration and separation of bioparticles. Ind Eng Chem Res. https://doi.org/10.1021/acs.iecr.9b00771
19. Cetin B, Öner SD, Baranoğlu B (2017) Modeling of dielectrophoretic particle motion: point particle versus finite-sized particle. Electrophoresis 38(11):1407–1418

20. Patki S et al (2012) Wireless EEG system with real time impedance monitoring and active electrodes. In: 2012 IEEE biomedical circuits and systems conference (BioCAS). IEEE
21. Phol HA (1978) Dielectrophoresis: the behavior of neutral matter in nonuniform electric field. Cambridge University Press, Cambridge
22. Huang Y, Holzel R, Pethig R, Wang X-B (1992) Differences in the AC electrodynamics of viable and non-viable yeast cells determined through combined dielectrophoresis and electrorotation studies. Phys Med Biol 37:1499
23. Buyukkockak S, Ozer MB, Cetin B (2017) Numerical modeling of ultrasonic particle manipulation for microfluidic applications. Microfluid Nanofluid 17:1025–1037
24. Srivastava SK et al (2008) Dielectrophoretic characterization of erythrocytes: positive ABO blood types. Electrophoresis 29(24):5033–5046
25. Kang Y et al (2008) DC-dielectrophoretic separation of biological cells by size. Biomed Microdevices 10(2):243–249
26. Chen KP et al (2009) Insulator-based dielectrophoretic separation of small particles in a sawtooth channel. Electrophoresis 30(9):1441–1448